doi:10.2533/chimia.2009.714 Chimia 63 (2009) 714–720 © Schweizerische Chemische Gesellschaft

Fluorescent Probes and Labels for Cellular Imaging

Christoph J. Fahrni*

Abstract: Metal-responsive fluorescent indicators are powerful tools for visualizing trace metals with subcellular resolution. By taking advantage of the diverse photophysical properties of organic fluorophores, metal ion-selective fluorescent indicators have been rationally designed and tailored towards cellular applications. This review summarizes challenges associated with the probe design and describes recent efforts in our research group in developing selective and sensitive reagents for the detection of zinc and copper in mammalian cells.

Keywords: Excited state proton transfer · Imaging · Photoinduced electron transfer · Trace metals · X-ray fluorescence microscopy

Christoph J. Fahrni earned a master's degree in chemistry from the Federal Institute of Technology (ETH, Switzerland) and a PhD degree in chemistry from the University of Basel (Switzerland) under the guidance of Prof. Andreas Pfaltz. He simultaneously pursued studies in piano performance at the Conservatories of Zurich and Lucerne (Switzerland), where he earned a bachelor's and master's degree. After working as a postdoctoral fellow with Prof. Thomas O'Halloran at Northwestern University (Evanston, USA), he joined the School of Chemistry and Biochemistry at the Georgia Institute of Technology to pursue his independent career. His current research interests focus on the development of fluorescent probes and imaging methodologies for studying the physiology of trace metals in biological systems.

*Correspondence: Prof. Dr. C. J. Fahrni
Georgia Institute of Technology
School of Chemistry and Biochemistry, and Petit Institute for Bioengineering and Bioscience
901 Atlantic Drive
Atlanta, GA 30332-0400, USA
Tel.: +1 404 385 1164
Fax: +1 404 894 2295
E-mail: fahrni@chemistry.gatech.edu

1. Introduction

Approximately one third of all currently known proteins contain one or more metal cations in their active site. These metalloproteins serve a wide range of biological functions, including signal transduction, gene regulation, and catalysis.[1] While the role of metal cofactors in proteins and the underlying reaction mechanisms have been a longstanding theme in bioinorganic research, the question of how cells acquire, store, and regulate metal cations is a newer area that has only more recently moved into the spotlight. This trend has been particularly stimulated by the discovery that impaired metal transport and regulation are the cause of an increasing number of diseases, including hemochromatosis, Menkes syndrome, and Alzheimer's disease. At present, many of the molecular mechanisms of metal trafficking and the nature of the involved cellular structures and organelles which may act as transient storage places are elusive; however, only a detailed understanding of these processes can pave the way towards new therapies for diseases caused by a metal imbalance. In this context, the detection and visualization of subcellular metal pools is of vital importance. In light of the small size of subcellular structures and the low abundance of many of the relevant metal cations, this task poses significant analytical challenges.[2] Among possible imaging modalities that offer sufficient sensitivity, fluorescence microscopy based approaches are particularly attractive. Depending on the brightness of the fluorescent label, this low-cost technique is capable of visualizing biological processes even at the single molecule level.[3] To detect metal cations in their native biological environment, cells or tissues are incubated with a fluorescent indicator that passively diffuses across biological membranes and selectively binds and responds to the cation of interest. At present, fluorescent indicators have been developed for many biologically relevant metal cations, including calcium, magnesium, sodium, potassium, zinc, copper, and iron.[4] This review summarizes some of the challenges associated with the development of fluorescent indicators and describes recent efforts in our research group to design selective and highly sensitive reagents for the detection of zinc and copper in mammalian cells.

2. Fluorescence Switches as Cation-selective Indicators

2.1 *Optimizing the Contrast Ratio through Electron Transfer Tuning*

Fluorescent indicators can be categorized in switches that either increase or decrease their emission intensity or generate a visible spectral shift. While the limit of detection for all indicators depends on the thermodynamic affinity towards the metal cation of interest, the fluorescence contrast between the bound and the free form is equally important to guarantee a broad dynamic range. For example, if a 'switch-on' indicator exhibits substantial residual emission in the absence of analyte, a fluorescence micrograph would be compromised by undesired background fluorescence, thus limiting the detection sensitivity and potentially introducing artifacts. Although many guidelines for the design of metal-selective fluorescent probes have been established,[5] the attainable contrast ratio is typically difficult to predict, such that only a laborious trial and error approach may lead to improved properties. We recently devised a strategy that allows for the systematic optimization of the contrast ratio of fluorescent indicators.[6–9]

To best illustrate the underlying design approach, the following section briefly reviews the photophysical mechanism that is responsible for the metal cation-induced switching response.

The presumably largest class of indicators is based on an ultrafast intramolecular photoinduced electron transfer (PET) process to modulate the emission response.[5] This type of indicator is composed of a donor-spacer-acceptor (D-A) molecular architecture, where the electron-rich metal-coordinating Lewis base functions as the electron donor **D** and the fluorophore as the acceptor **A** (Fig. 1). Upon photoexcitation, the fluorophore **A*** exhibits dramatically different redox properties and can accept an electron from the donor moiety to form a radical ion pair ($A^{\bullet-}$–$D^{\bullet+}$). Because back electron transfer to the initial ground state species is typically a non-radiative process, in most cases PET leads to fluorescence quenching (Fig. 1a).[10] Upon coordination of a metal cation to the electron donor **D**, the PET process is rendered less favorably, and as a consequence, fluorescence quenching is reduced and the fluorescence output increased (Fig. 1b).

The magnitude of the emission increase is directly related to the relative rates of the PET processes in absence and presence of the metal cation. Because the metal cation does not directly interact with the fluorophore, only the emission intensity is altered but not the wavelength. At the same time, the sigma-bond spacer electronically decouples the quenching electron donor from the fluorophore, hence, the electron transfer reaction proceeds in the nonadiabatic regime and is best described by semiclassical Marcus theory.[11,12] Within this framework, the kinetics depends on the thermodynamic driving force of the ET reaction, the associated reorganization energy, and the electronic coupling between the excited fluorophore and the successor radical ion pair. The driving force of the ET reaction ($-\Delta G_{et}$) in turn depends on the ground state potentials of the electron donor $E(D^+/D)$ and acceptor $E(A/A^-)$ and the excited state energy ΔE_{00} of the fluorophore, as expressed by the Rehm-Weller Eqn. (1).[13]

$$\Delta G_{et} = E(D^+/D) - E(A/A^-) - \Delta E_{00} - w_p \quad (1)$$

The work term w_p describes the Coulombic stabilization energy of the formed radical ion pair and is typically small in polar solvents such as water.[10] Hence, Eqn. (1) captures the essential photophysical parameters that directly affect the electron transfer kinetics and thus the switching response and contrast ratio of the indicator.

While the donor potential $E(D^+/D)$ is determined by the choice of ligand utilized as the cation-recognition unit, the excited state energy ΔE_{00} and the acceptor potential $E(A/A^-)$ inherently depend on the fluorophore structure, making it essentially impossible to selectively tune one parameter without changing the other. Detailed photophysical and quantum chemical studies of 1,3,5-triarylpyrazoline fluorophores revealed that this compound class makes a welcome exception.[6,7] The π-system responsible for the spectral properties of this fluorophore is composed of the central pyrazoline unit and the aryl-substituents attached in the 1- and 3-positions of the ring (Fig. 2). The aryl group in the 5-position of the pyrazoline ring is electronically decoupled from the fluorophore π-system, and only indirectly influences the emission response, for example through PET quenching with an electron-rich cation-binding unit. Because the LUMO is predominantly localized on the 3-aryl ring, substituents attached to the 1-aryl ring exert only a small influence on the acceptor potential $E(A/A^-)$ but large changes in the excited state energy ΔE_{00} of the fluorophore. This rather unusual property allows for selective tuning of ΔE_{00} while keeping $E(A/A^-)$ at the same level, and thus for predictably adjusting the PET driving force according to Eqn. (1) to offset the donor potential $E(D^+/D)$ of a given cation receptor.

To test this optimization strategy, we synthesized a series of pH-responsive pyrazoline derivatives **1a-f** containing an increasing number of fluoro-substituents attached on the 1-aryl ring. As illustrated with the data compiled in Table 1, the excited state energy gradually increases with the number of fluoro-substituents, while the reduction potential remains centered at –2.21 ± 0.03 V. As a consequence, the electron transfer driving force $-\Delta G_{et}$ is also rendered more favorable, which in turn leads to a decreased quantum yield under neutral conditions. In acidic solution, the

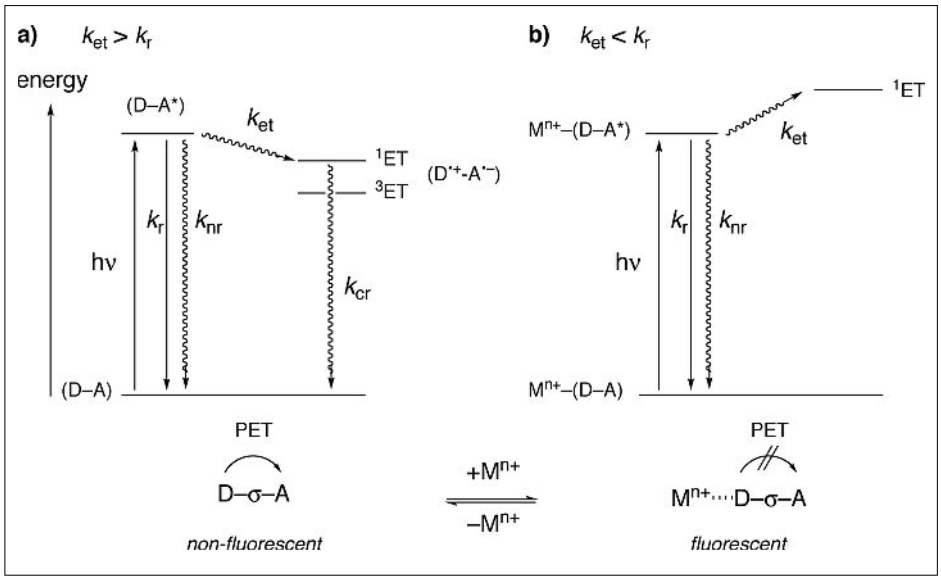

Fig. 1. Simplified Jablonski diagram illustrating the emission response of fluorescent metal indicators based on photoinduced electron transfer (PET) switching. a) In absence of the metal cation M^{n+}, electron transfer from the donor D to the excited fluorophore (A*) is thermodynamically favorable. The rate of electron transfer k_{et} is faster than the rate for radiative deactivation (k_r), resulting in emission quenching. b) Metal coordination to the electron donor D decreases the driving force for PET, and slows down the electron transfer process. Radiative deactivation favorably competes with PET, and the fluorescence is switched on.

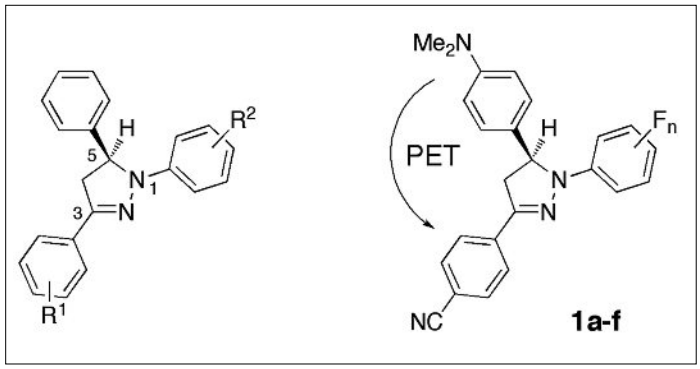

Fig. 2. Fluorescent indicators based on photoinduced electron transfer (PET) switching using 1,3,5-triarylpyrazolines as fluorophore platform.

Table 1. Photophysical Data for Pyrazoline Derivatives **1a–f**.[a]

compd	R	ΔE_{00} [b] (eV)	$E(A/A^-)$ [c] (V)	ΔG_{et} [d] (V)	Φ_f [e]	Φ_f' [f]	f_e [g]
1a	H	2.79	–2.26	–0.13	0.014	0.49	35
1b	3-F	2.86	–2.23	–0.23	0.0076	0.61	80
1c	4-F	2.79	–2.26	–0.12	0.016	0.51	33
1d	2,5-F_2	2.93	–2.21	–0.31	0.0038	0.63	166
1e	2,3,5,6-F_4	3.15	–2.23	–0.46	0.0033	0.71	215
1f	2,3,4,5,6-F_5	3.19	–2.18	–0.56	0.0017	0.68	400

[a]Data from ref. [6]. [b]Zero-zero transition energy of the emissive state. [c]Reduction half-wave potential in acetonitrile 0.1 Bu_4NPF_6 vs $Fc^{+/0}$ at 298 K. [d]Electron transfer free energy calculated according to Eqn. (1) with w_p = –0.045 eV. [e]Quantum yield in neutral acetonitrile. [f]Quantum yield in 10 mM trifluoroacetic acid/acetonitrile. [g]Fluorescence enhancement factor upon acidification $f_e = \Phi_f'/\Phi_f$.

Table 2. Theoretical Hammett substituent constants σ^c for selected mono- and polysubstituted fluorobenzenes.[a]

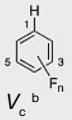

Substituent	V_c [b] (au)	σ^c [c]
H	–14.77568	0.03
2-F	–14.76462	0.28
3-F	–14.76191	0.34
4-F	–14.76832	0.20
2,4-F_2	–14.75760	0.44
3,5-F_2	–14.74826	0.65
2,5-F_2	–14.75083	0.59
2,4,5-F_3	–14.74482	0.73
2,3,4,5-F_4	–14.73391	0.98
2,3,5,6-F_4	–14.72994	1.07
2,3,4,5,6-F_5	–14.72481	1.19

[a]Data from ref. [9]. [b]Electrostatic potential *V* at nucleus C1 in atomic units according to Eqn. (2) (numbering scheme shown above). [c]Theoretical substituent constant based on the linear relationship $\sigma^c = (V_C + 14.777)/0.044$, see original reports for details.[9,14]

aniline nitrogen is protonated and becomes electrochemically inactive. Under these conditions, the PET process is effectively inhibited, yielding an optimized fluorescence enhancement of 400-fold.

2.2 *Linear Free Energy Relationships for Predicting the Electron Transfer Thermodynamics in 1,3,5-Triarylpyrazolines*

The observed systematic changes of the electron transfer parameters in response to the substituents attached to the 1-aryl ring prompted us to investigate, whether the photophysical properties of 1,3,5-triaryl pyrazolines might be predicted based on linear free energy relationships (LFERs). For this purpose, we correlated quantum chemical parameters obtained from density functional theory calculations, specifically the gas phase LUMO energies, the adiabatic electron affinities, and the vertical excitation energies, with the corresponding experimental data.[6] The LFERs yielded an average unsigned error of less than 0.03 eV over 20 structurally distinct pyrazoline fluorophores with excellent correlation coefficients of $r > 0.995$.

Encouraged by these results and the observation that the excited state energy and acceptor potential are strongly influenced by the nature of the substituents R^1 and R^2, we envisioned that a set of two Hammett constants might already be sufficient to capture the electronic contribution of each aryl ring and thus to predict the electron transfer parameters for a particular pyrazoline derivative. For this purpose, we synthesized and experimentally characterized the acceptor potentials and excited state energies of another small fluorophore library composed of 20 distinct polyfluoro-substituted 1,3-diaryl-5-phenyl-pyrazolines.[9] The corresponding Hammett constants of polyfluorinated aromatics were derived based on the theoretical electrostatic potentials at the nuclei (EPN) of carbon atoms. Galabov *et al.* recently demonstrated that this quantum chemical parameter is an excellent reactivity descriptor of substituted benzenes.[14] The electrostatic potential V_A at the nucleus of interest (A) in a molecule containing N nuclei can be calculated based on the molecular electrostatic potential by dropping the contribution due to the charge Z_A on nucleus A according to Eqn. (2):

$$V_A = \sum_{i \neq A}^{N} \frac{Z_i}{|R_i - R_A|} - \int \frac{\rho(r')}{|R_A - r'|} d^3r' \qquad (2)$$

where Z_i and R_i are the charge and radius vectors of the nucleus i, ρ is the electron-density of the molecule, and *r*' is a dummy integration variable.[15] Taking advantage of the fact that the theoretically estimated EPN values based on Eqn. (2) correlated linearly with the experimental Hammett constants σ^0 of 29 substituted benzenes (r = 0.993), we derived computational constants σ^c for the respective mono- and polyfluorosubstituted benzenes (Table 2).[9] These values in combination with the experimental data served then as an LFER training set to determine the corresponding regression parameters, which in turn were utilized to predict the excited state energies and acceptor potentials of five pyrazoline derivatives that were not included in the initial training set.[9] Fig. 3 illustrates the correlation results for the combined PET parameters, $\Delta E_{00} + E(A/A^-)$, in the form of a 3D-plot. The training set data points are represented as black spheres, the regression plane is shown as a semi-transparent surface, and the test data are plotted in red. The plot reveals evenly spread data points without apparent systematic deviation for both the training set and the test set of compounds. Based on this LFER, the combined PET parameters of the test compounds were predicted with a mean unsigned error of 0.046 eV. While the prediction of the PET parameters is obviously limited to the experimental conditions utilized to calibrate the training set LFER, the outlined approach offers a valuable guideline for optimizing the performance and contrast ratio of cation-responsive fluorescent probes.

2.3 *Fluorescent Indicators for Cellular Copper*

Over the past decade, the identification of genes coding for proteins involved in copper-uptake, transport, and regulation clearly underscored the importance of copper for human health.[16] Given the reducing environment of the cytosol,[17] the bulk of intracellular copper is present in its monovalent oxidation state. To probe the subcellular localization of copper in mammalian cells, we developed the membrane-permeable Cu(I)-responsive fluorescent indicator **CTAP-1**, composed of a pyrazoline fluorophore and a thiazo crown ether moiety as the cation receptor (Fig. 4).[8] Upon saturation with Cu(I), the probe produced a 4.6-fold emission enhancement at 480 nm, which was not compromised by Ca(II) or Mg(II), both of which are present at significantly higher concentrations inside cells. The indicator

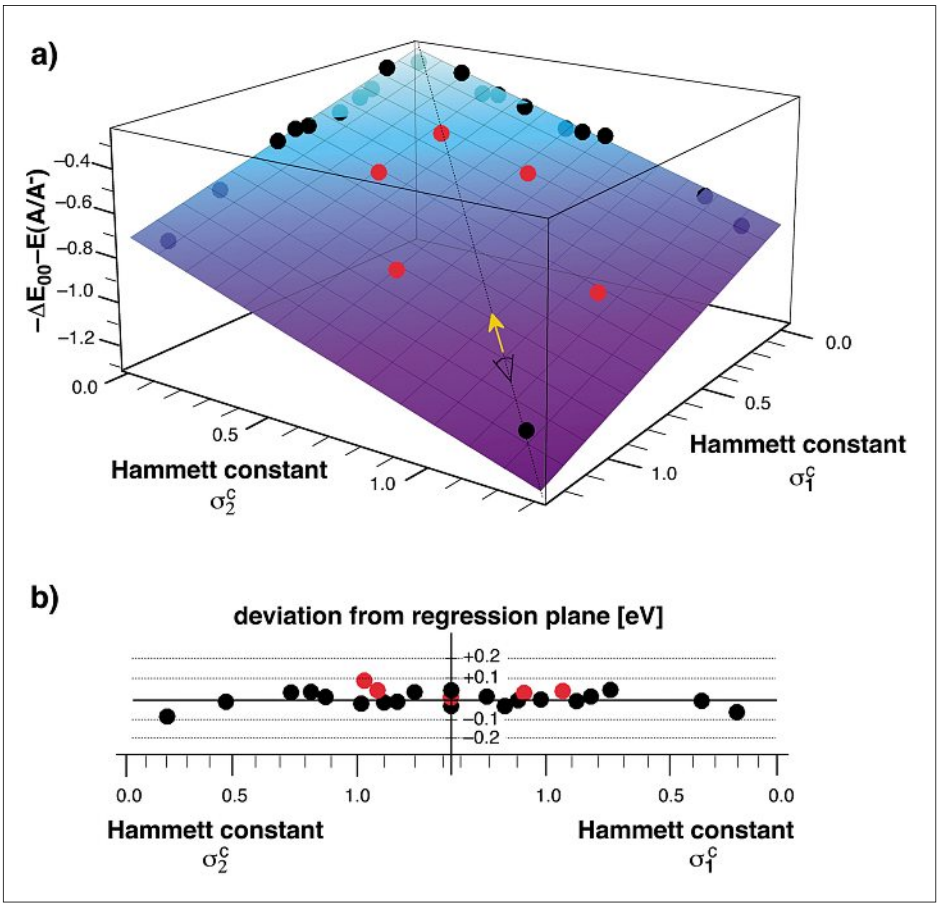

Fig. 3. Linear free energy relationship (LFER) of computational Hammett constants (Table 2) and the combined experimental excited state energy ΔE_{00} and reduction potential $E(A/A^-)$. a) 3D-plot of the regression plane and experimental data points of the LFER training set. b) Projection of above regression plane along the diagonal vector shown in yellow. Reprinted with permission from ref. [9]. Copyright 2009 Royal Society of Chemistry.

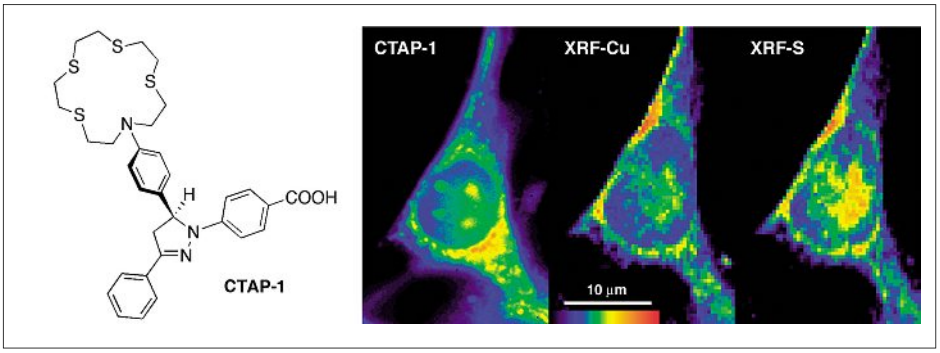

Fig. 4. Subcellular topography of copper in a NIH 3T3 mouse fibroblast cell visualized by optical and X-ray fluorescence microscopy. Left micrograph: False color fluorescence micrograph of a cell incubated with CTAP-1, a Cu(I)-responsive fluorescent indicator. Middle and right micrograph: X-ray fluorescence elemental maps for copper and sulfur of the same specimen after in-air drying (raster scan with 10 keV excitation). Reprinted with permission from ref. [8]. Copyright 2005 National Academy of Sciences.

revealed a copper-dependent perinuclear staining pattern in 3T3 mouse fibroblast cells. The subcellular topography of copper, which appeared to be predominantly localized in the Golgi apparatus and mitochondria, was independently visualized by synchrotron-based X-ray fluorescence microscopy, a microanalytical technique capable of imaging trace elements with submicron resolution (Fig. 4).[18,19] Furthermore, X-ray absorption measurements at several cellular locations revealed a near-edge structure (XANES) that is consistent with monovalent copper in a low-coordinate environment.[8] Current efforts focus on improving the contrast ratio of Cu(I)-responsive probes based on above outlined tuning strategy.

3. Ratiometric Zinc(II)-Selective Fluorescent Indicators

Due to the heterogeneous cellular environment, the concentration of a fluorescent indicator might vary not only from cell to cell, but also within different regions of the cytoplasm. For this reason, fluorescent indicators that undergo an emission enhancement can be only utilized to determine qualitative changes in metal ion concentrations, whereas quantitative measurements are difficult to achieve inside cells. Fluorescent probes that exhibit a spectral shift rather than an intensity change upon analyte binding offer a workaround to this problem, since the free probe can be chromatically distinguished from the analyte bound form.[20] By measuring the ratio R of fluorescence intensities at two distinct excitation or emission wavelengths, the probe response can be quantitatively related to the metal ion concentration $[M^{n+}]$ according to Eqn. (3).

$$[M^{n+}] = K_d \left(\frac{R - R_{min}}{R_{max} - R}\right)\left(\frac{S_f}{S_b}\right) \qquad (3)$$

where K_d is the dissociation constant of the metal-probe complex (with 1:1 stoichiometry), R_{min} and R_{max} are the minimum and maximum intensity ratios for the free and saturated probe, and S_f and S_b are instrument dependent calibration constants.[20] With this method, intensity differences due to uneven intracellular distribution, photodegradation, or instrument dependent fluctuations are cancelled out. The instrument parameters S_f and S_b as well as the limiting intensity ratios R_{min} and R_{max} can be determined through calibration with metal-buffered solutions.

3.1 *Cation-Induced Inhibition of Excited State Intramolecular Proton Transfer*

There is increasing evidence that intracellular zinc storage sites are presumably an integral component of the homeostatic machinery regulating cellular zinc concentrations.[21] To build a ratiometric indicator for exploring these zinc stores, we designed spectral switches based on excited state intramolecular proton transfer (ESIPT),[22–26] a photophysical process observed in a range of benzazole derivatives containing an intramolecular hydrogen bond. As shown in Fig. 5, upon photoexcitation the X–H proton in this type of molecule is rendered acidic and moves to the nearby benzazole nitrogen atom. The

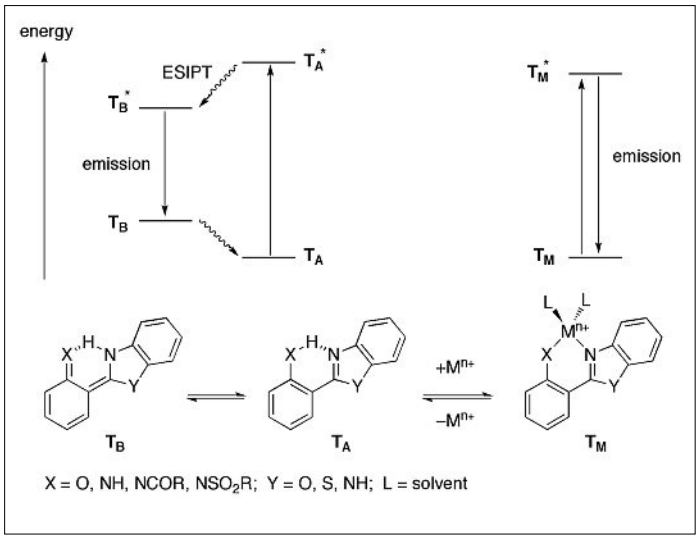

Fig. 5. Jablonski diagram illustrating the metal-dependent spectral response of a fluorescent indicator undergoing excited state intramolecular proton transfer (ESIPT). Left: In absence of a metal cation M^{n+}, the excited benzazole T_A^* undergoes rapid intramolecular proton transfer to yield the phototautomer T_B^* which emits with a large Stokes shift. Right: Metal coordination replaces the proton responsible for ESIPT, and restores normal emission at higher energy from a local excited state (T_M^*).

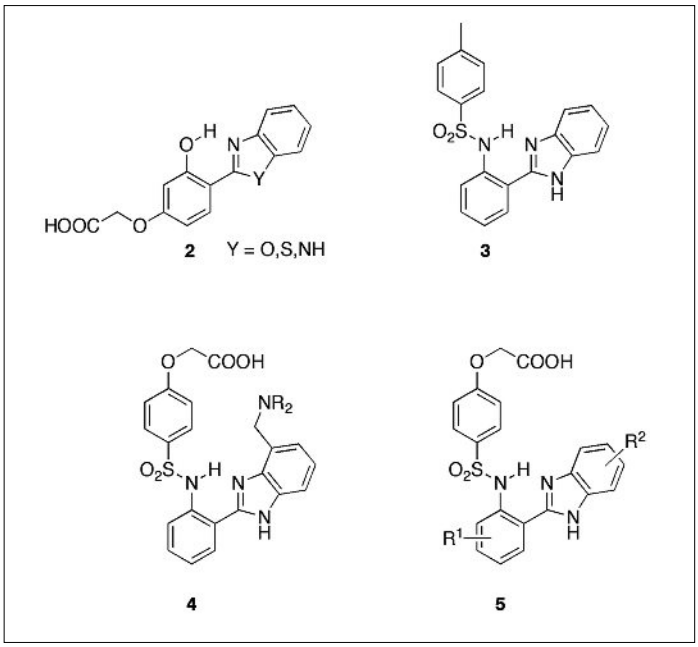

Fig. 6. Ratiometric Zn(II)-selective fluorescent indicators based on intramolecular proton transfer (ESIPT). Coordination of Zn(II) replaces the intramolecular H-bond and inhibits ESIPT, yielding a strongly blue-shifted fluorescence emission.

formed tautomer T_B^* subsequently emits a photon and equilibrates back to the more stable ground-state form (T_A). Because the phototautomer is more stable in the excited-state but not the ground-state, the Stokes shift of the fluorescence emission is unusually large. We hypothesized that coordination of Zn(II) would replace the proton involved in ESIPT, and therefore produce a significantly blue-shifted emission suitable for ratiometric detection.

As a first step towards implementing this design concept, we explored the photophysical properties of a series of water-soluble 2-(2'-hydroxyphenyl)-benzazole derivatives **2** under simulated physiological conditions (Fig. 6).[22] Coordination to Zn(II) indeed yielded the expected blue shift; however, the system also displayed a pronounced sensitivity towards the polarity of the environment. Careful analysis revealed that this polarity responsiveness is due to the presence of a *trans*-rotamer that cannot undergo ESIPT. To shift the ground-state equilibrium towards the ESIPT-capable *cis*-rotamer, the hydroxy group was replaced with a sulfonamide moiety. Rigorous characterization of **3** using a combination of X-ray crystallography, quantum chemical calculations, as well as steady-state and time-resolved fluorescence and absorption spectroscopy unequivocally demonstrated exclusive formation of the phototautomer and complete absence of the solvent-dependent dual emission behavior.[23] These studies provided a solid basis for the design of a sensor family **4** with tunable affinity and high selectivity towards Zn(II).[24] Due to electronic decoupling of the pendant chelating groups and the fluorophore π-system, the sensor family exhibits uniform spectral characteristics and can be used with a single filter set. The sensors cover a broad dynamic range suitable for millimolar to picomolar Zn(II) concentration measurements.[24] In an effort to tune the excitation and emission spectra as well as the pK_a of the sulfonamide nitrogen, we synthesized and characterized a series of substituted 2-(2'-arylsulfonamidophenyl) benzimidazole derivatives **5**.[25,26] Electron-donating substituents attached in the *para*-position relative to the sulfonamide nitrogen yielded a red-shifted emission, while *meta*-substitution produced a blue-shift. Detailed photophysical and quantum chemical studies revealed that the surprisingly divergent emission shift was due to a differential change in the HOMO and LUMO energies of the ESIPT phototautomer.[26]

3.2 *Ratiometric Indicators with Enhanced Two-Photon Cross Section and Brightness*

Two-photon excitation microscopy (TPEM) is a three-dimensional imaging technique that has found widespread use in biological research.[27,28] By using an ultrafast pulsed laser as the excitation source, two photons are absorbed simultaneously by the fluorophore. Because this process scales with the squared intensity of the laser pulse, excitation occurs only within a spatially confined volume at the focal point of the microscope objective. Compared to conventional fluorescence microscopy, TPEM offers reduced phototoxicity, improved depth penetration, and negligible background fluorescence.[28] Most fluorophores that are used as labels or fluorescent probes have been adopted from linear microscopy and are not optimized for two-photon excitation. To develop a Zn(II)-responsive fluorescent indicator with optimized nonlinear optical properties for TPEM, we explored the utility of donor-acceptor architectures such as the oxazole derivative **6** where the metal-ion coordinates to the acceptor rather than donor site of the fluorophore.[29] Zn(II)-binding to **6** resulted in a significant increase of the two-photon absorption cross-section (δ) and fluorescence brightness (ηδ). The fluorophore also showed a strong shift of the emission peak upon saturation with Zn(II), rendering the proposed approach suitable for two-photon excited emission ratiometric sensing (Fig. 7). Because the two photon absorption cross section of **6** is negligible above 800 nm but strongly enhanced upon Zn(II) saturation, the indicator can be also used in 'turn on' mode, thus offering an excellent contrast ratio with >10,000 fold emission increase in this spectral region.

4. Targeted Fluorescent Labeling of Biomolecules

4.1 *Fluorogenic Labels Based on $^3(n,\pi^*)$–$^1(\pi,\pi^*)$ Excited State Inversion*

Chemoselective ligation reactions represent a powerful approach for labeling

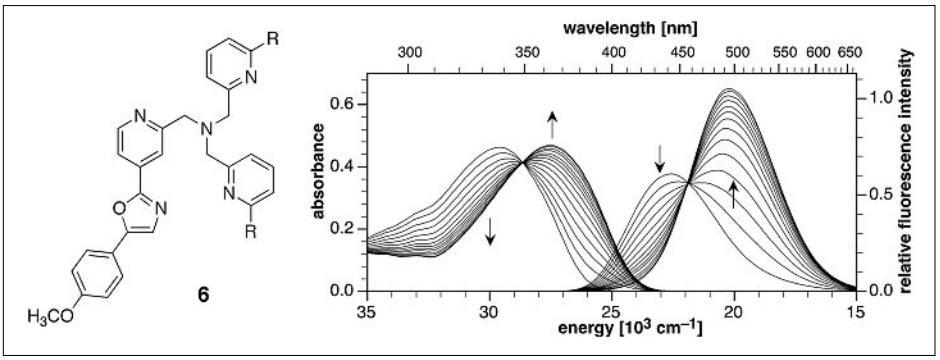

Fig. 7. Spectral response (absorption and fluorescence) of a ratiometric Zn(II)-selective fluorescent indicator for nonlinear microscopy. Coordination of Zn(II) to the pyridine groups of indicator **6** results in an increased excited state charge transfer, which in turn is responsible for an enhanced two-photon absorption cross section and a strong spectral shift of the peak emission wavelength. Reprinted with permission from ref. [29]. Copyright 2007 American Chemical Society.

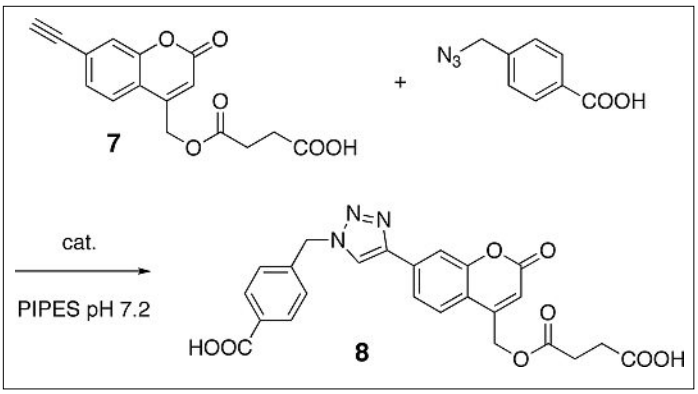

Scheme. A fluorogenic probe (**7**) for the copper-catalyzed azide-alkyne ligation. The strong fluorescence increase upon formation of the triazole **8** is due to an inversion of the energy ordering of the quenching triplet $^3(n,\pi^*)$ state and the emissive singlet $^1(\pi, \pi^*)$ state.

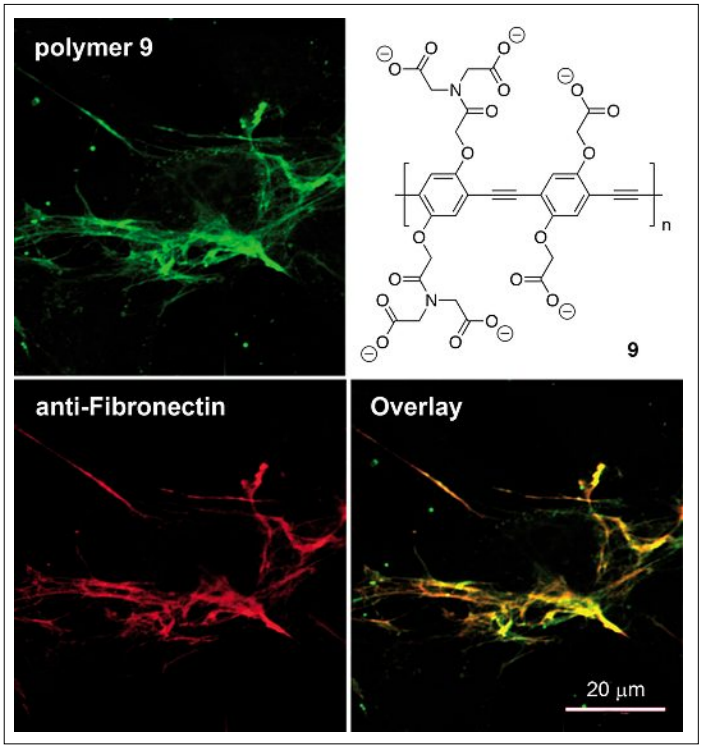

Fig. 8. Molecular recognition based on low-affinity polyvalent interactions. Top row: Fluorescence micrograph showing the selective binding of anionic polymer **9** to extracellular fibronectin fibrils of live NIH 3T3 fibroblast cells. Bottom row: Immunofluorescence colocalization of **9** with an antibody specific for fibronectin. Areas of colocalization are revealed in orange/yellow in the overlay. Reprinted with permission from ref. [32]. Copyright 2008 American Chemical Society.

proteins or small molecules in a biological environment. To significantly reduce the background fluorescence of the unreacted fluorescence label we developed a fluorogenic probe **7** that is activated by copper(I)-catalyzed click chemistry (Scheme),[30] a highly versatile bio-orthogonal and chemoselective ligation reaction.[31] The electron-donating properties of the triazole ring in **8** that is formed in the coupling reaction, invokes an inversion of the energy ordering of the emissive singlet $^1(\pi,\pi^*)$ and non-emissive triplet $^3(n,\pi^*)$ excited states. As a consequence, non-radiative deactivation through fast intersystem crossing from $^1(\pi,\pi^*)$ to $^3(n,\pi^*)$ was effectively suppressed, which in turn resulted in a 18-fold increase of the quantum yield.[31] The rapid kinetics of the ligation reaction renders the probe attractive for a wide range of applications in biology, analytical chemistry, and materials science.

4.2 *Molecular Recognition Based on Low-Affinity Polyvalent Interactions*

In an entirely different approach towards biolabeling, we explored molecular recognition in the complex environment of the extracellular matrix using fluorescent polymers bearing either cationic alkylammonium or anionic carboxylate side chains.[32] While incubation of live NIH 3T3 fibroblast cells with the cationic polymer yielded perinuclear punctate staining reminiscent of endocytotic vesicles, the carboxylated polymer **9** revealed a characteristic filamentous staining pattern (Fig. 8). Histochemical and immunofluorescence studies demonstrated that the anionic poly(*p*-phenyleneethynylene) polymer **9** selectively binds to fibronectin fibrils of the extracellular matrix. An *in vitro* binding study revealed a dissociation constant of approximately 100 nM for the fibronectin-polymer complex. Both polymers displayed bright two-photon excited emission as well as low toxicity, rendering them well suited for live cell imaging studies. Our studies demonstrated that selective molecular recognition of biomolecules in the complex environment of the extracellular matrix can be achieved by taking advantage of non-specific low-affinity polyvalent interactions.

Conclusions

Metal-responsive fluorescent indicators have become invaluable tools in the diverse instrument arsenal of the cell biologist in addressing important questions pertaining to metal storage, trafficking, and cellular homeostasis. By exploiting the diverse photophysics of organic fluorophores, synthetic probes selective towards

any of the biologically relevant metal cations can be designed and their properties tailored towards specific applications. The combination of various imaging modalities, including linear and nonlinear fluorescence microscopy, electron microscopy, and scanning X-ray fluorescence microprobe analyses, offers particularly exciting opportunities to gain new insights into the distribution and speciation of metal cations at the subcellular level.

Acknowledgements

Financial support by the National Institutes of Health (GM067169, GM072021, DK68096) for the research described in this article is gratefully acknowledged.

Received: June 15, 2009

[1] R. R. Crichton, 'Biological Inorganic Chemistry: An Introduction', Elsevier Science, Amsterdam, **2008**.
[2] R. McRae, P. Bagchi, S. Sumalekshmy, C. J. Fahrni, *Chem. Rev.* **2009**, *109*; doi:10.1021/cr900223a.
[3] T. Yanagida, Y. Ishii, 'Single Molecule Dynamics in Life Science', Wiley-VCH, Weinheim, **2009**.
[4] D. W. Domaille, E. L. Que, C. J. Chang, *Nat. Chem. Biol.* **2008**, *4*, 168.
[5] A. P. de Silva, H. Q. N. Gunaratne, T. Gunnlaugsson, A. J. M. Huxley, C. P. McCoy, J. T. Rademacher, T. E. Rice, *Chem. Rev.* **1997**, *97*, 1515.
[6] J. Cody, S. Mandal, L. Yang, C. J. Fahrni, *J. Am. Chem. Soc.* **2008**, *130*, 13023.
[7] C. J. Fahrni, L. C. Yang, D. G. VanDerveer, *J. Am. Chem. Soc.* **2003**, *125*, 3799.
[8] L. Yang, R. McRae, M. M. Henary, R. Patel, B. Lai, S. Vogt, C. J. Fahrni, *Proc. Natl. Acad. Sci. USA* **2005**, *102*, 11179.
[9] M. Verma, A. F. Chaudhry, C. J. Fahrni, *Org. Biomol. Chem.* **2009**, *7*, 1485.
[10] G. J. Kavarnos, 'Fundamentals of Photoinduced Electron Transfer', VCH Publishers, New York, **1993**.
[11] R. A. Marcus, N. Sutin, *Biochim. Biophys. Acta* **1985**, *811*, 265.
[12] G. L. Closs, J. R. Miller, *Science* **1988**, *240*, 440.
[13] D. Rehm, A. Weller, *Isr. J. Chem.* **1970**, *8*, 259.
[14] B. Galabov, S. Ilieva, H. F. Schaefer, *J. Org. Chem.* **2006**, *71*, 6382.
[15] P. Politzer, J. S. Murray, *Theor. Chem. Acc.* **2002**, *108*, 134.
[16] B.-E. Kim, T. Nevitt, D. J. Thiele, *Nat. Chem. Biol.* **2008**, *4*, 176.
[17] C. T. Dooley, T. M. Dore, G. T. Hanson, W. C. Jackson, S. J. Remington, R. Y. Tsien, *J. Biol. Chem.* **2004**, *279*, 22284.
[18] C. J. Fahrni, *Curr. Opin. Chem. Biol.* **2007**, *11*, 121.
[19] R. McRae, B. Lai, S. Vogt, C. J. Fahrni, *J. Struct. Biol.* **2006**, *155*, 22.
[20] G. Grynkiewicz, M. Poenie, R. Y. Tsien, *J. Biol. Chem.* **1985**, *260*, 3440.
[21] D. J. Eide, *Biochim. Biophys. Acta* **2006**, *1763*, 711.
[22] M. M. Henary, C. J. Fahrni, *J. Phys. Chem. A* **2002**, *106*, 5210.
[23] C. J. Fahrni, M. M. Henary, D. G. VanDerveer, *J. Phys. Chem. A* **2002**, *106*, 7655.
[24] M. M. Henary, Y. Wu, C. J. Fahrni, *Chem. Eur. J.* **2004**, *10*, 3015.
[25] M. M. Henary, Y. Wu, J. Cody, S. Sumalekshmy, J. Li, S. Mandal, C. J. Fahrni, *J. Org. Chem.* **2007**, *72*, 4784.
[26] Y. Wu, P. V. Lawson, M. M. Henary, K. Schmidt, J.-L. Brédas, C. J. Fahrni, *J. Phys. Chem. A* **2007**, *111*, 4584.
[27] A. Diaspro, G. Chirico, M. Collini, *Q. Rev. Biophys.* **2005**, *38*, 97.
[28] C. J. Fahrni in 'Reviews in Fluorescence 2007', Ed. C. D. Geddes, Springer, New York, **2009**, p 249.
[29] S. Sumalekshmy, M. M. Henary, N. Siegel, P. V. Lawson, Y. Wu, K. Schmidt, J.-L. Brédas, J. W. Perry, C. J. Fahrni, *J. Am. Chem. Soc.* **2007**, *129*, 11888.
[30] Z. Zhou, C. J. Fahrni, *J. Am. Chem. Soc.* **2004**, *126*, 8862.
[31] V. V. Rostovtsev, L. G. Green, V. V. Fokin, K. B. Sharpless, *Angew. Chem. Int. Ed.* **2002**, *41*, 2596.
[32] R. L. McRae, R. L. Phillips, I. B. Kim, U. H. F. Bunz, C. J. Fahrni, *J. Am. Chem. Soc.* **2008**, *130*, 7851.